ISSN 0021-3640, JETP Letters, 2023, Vol. 117, No. 5, pp. 392–399. © Pleiades Publishing, Inc., 2023.
Russian Text © The Author(s), 2023, published in Pis'ma v Zhurnal Eksperimental'noi i Teoreticheskoi Fiziki, 2023, Vol. 117, No. 5, pp. 389–396.

BIOPHYSICS

Backscattering of Infrared Radiation by a Model Multilayer Biological Tissue

Yu. A. Zhavoronkov[a],*, S. V. Ul'yanov[a],, A. Yu. Valkov[a,b],***, and V. L. Kuzmin[b],****

[a] *St. Petersburg State University, St. Petersburg, 198504 Russia*

[b] *Peter the Great St. Petersburg Polytechnic University, St. Petersburg, 195251 Russia*

**e-mail: zhavoronkov95@gmail.com*

***e-mail: ulyanov_sv@mail.ru*

****e-mail: alexvalk@mail.ru*

*****e-mail: kuzmin_vl@mail.ru*

Received January 25, 2023; revised January 25, 2023; accepted January 30, 2023

The intensity of backscattering of near infrared laser radiation has been calculated for a multilayer biological tissue simulating the human head as a function of the distance between a source and a detector of radiation that are located on the head. The iterative solution of the Bethe–Salpeter equation has been represented as a series in scattering orders. A modification of the known Monte Carlo method for photon transport in multilayer tissues has been proposed to accelerate calculations. It has been shown that the resulting dependences of the backscattering intensity change significantly under the variation of the optical properties of the biological tissue, primarily in the case of penetration of blood to the cerebrospinal fluid layer. This can be used to develop optical methods for diagnosis of traumatic injuries of biological tissues.

DOI: 10.1134/S0021364023600180

INTRODUCTION

Interest in optical methods for medical diagnostics is currently growing [1–5] primarily because inexpensive noninvasive optical methods, which can be easily applied under "tough" conditions, can provide critically important information on the state of deep layers of biological tissues. Because of a low absorption coefficient of biological tissues in the near infrared region, diffusion spectroscopy methods were developed to detect injuries of the skin and hypodermis, traumas of soft tissues and the brain, venous injuries, and pressure ulcers [3, 5–9]. A biological tissue can be exposed to infrared radiation of different types such as continuous radiation [10–13], short pulses [14–17], and waves with various modulations [14, 18, 19].

In this work, an approach is developed to obtain information on the state of a multilayer biological tissue from data on the backscattering of continuous infrared laser radiation. We apply it to the model of the human head. To adequately use the data on the backscattering of infrared laser radiation in medical diagnostics, it is necessary to take into account the layered structure of the head, at least the skull and brain [12, 13, 20, 21]. Since the optical properties of biological tissues of the human head very strongly vary from the outer layer to the inner one, the layered structure of the head should be accurately simulated for the more accurate interpretation of backscattering data [6].

We calculated the dependence of the intensity of backscattered laser radiation on the distance along the surface of the head between the source and detector, which are located directly on the head. The human head is simulated as a four-layer medium consisting of the skin, skull, cerebrospinal fluid (CSF), and brain. To describe radiation transport in a randomly inhomogeneous medium, we used the iterative solution of the Bethe–Salpeter equation. The resulting series is the expansion in scattering orders. Each term of the series is a multiple integral, which is calculated using the Monte Carlo method. The performed calculations make it possible to reveal how the dependence of the backscattered radiation intensity on the source–detector distance changes under the variation of the physical and geometric parameters of the model. The effect of the penetration of blood to the cerebrospinal fluid, which often occurs upon traumatic injuries of the head, and the effect of the thickness of skull, which noticeably varies over the surface of the head, on the optical characteristics of the cerebrospinal fluid layer are of the most interest.

DESCRIPTION OF RADIATION TRANSPORT

We simulated the backscattering of infrared radiation for a layered scattering medium filling the half-space $z > 0$. The angle of incidence of a plane wave on

the medium measured from the outer normal is denoted as θ_i, and θ_f is the backscattering angle measured from the same normal at which the wave undergoing multiple scattering leaves the medium. Reflections and refractions of waves at the interfaces between the layers are neglected. For the backscattered field, we used the Fraunhofer approximation, in which the far field is the product of a spherical wave and a plane wave directed to the observation point [13, 22]. In this case, the main incoherent part of the backscattering intensity can be represented up to a constant dimensional factor in the form [13, 22–24]

$$J(s_i, s_f) = 4\pi\int_0^\infty dz_1 \int_{z_2>0} dr_2 \Gamma(\mathbf{r}_2, \mathbf{r}_1|\mathbf{k}_f, \mathbf{k}_i) \times \exp\left(-\mu(s_f z_2 + s_i z_1)\right). \quad (1)$$

Here, $s_i = 1/\cos\theta_i$, $s_f = 1/\cos\theta_f$, μ is the extinction coefficient, the exponential factor is due to the damping of the plane wave according to the Burger–Lambert–Beer law on the path from the boundary of the medium to the point of the first scattering event and on the path from the point of the last scattering event to the boundary of the medium, $\Gamma(\mathbf{r}_2, \mathbf{r}_1|\mathbf{k}_f, \mathbf{k}_i)$ is the coherence function describing radiation transport from the point $\mathbf{r}_1$ to the point $\mathbf{r}_2$ in the randomly inhomogeneous medium including all scattering orders, and $\mathbf{k}_i$ and $\mathbf{k}_f$ are the wave vectors of the wave reaching the point $\mathbf{r}_1$ and the multiply scattered wave leaving the medium from the point $\mathbf{r}_2$, respectively.

Radiation transport in a randomly inhomogeneous medium can be described by the Bethe–Salpeter equation [22, 23]

$$\Gamma(\mathbf{r}_2, \mathbf{r}_1|\mathbf{k}_f, \mathbf{k}_i) = \mu_s p\left(\mathbf{k}_f - \mathbf{k}_i\right)\delta(\mathbf{r}_2 - \mathbf{r}_1) + \mu_s\int d r_3 p\left(\mathbf{k}_f - \mathbf{k}_{23}\right)\Lambda(\mathbf{r}_2 - \mathbf{r}_3)\Gamma(\mathbf{r}_3, \mathbf{r}_1|\mathbf{k}_{23}, \mathbf{k}_i). \quad (2)$$

Here, $\mathbf{k}_{ij} = k_0\mathbf{r}_{ij}/r_{ij}$ is the wave vector directed from point $\mathbf{r}_j$ to point $\mathbf{r}_i$, where $k_0 = 2\pi/\lambda$ is the wavenumber in vacuum, λ is the wavelength, and $\mathbf{r}_{ij} = \mathbf{r}_i - \mathbf{r}_j$, and $\Lambda(r) = r^{-2}\exp(-\mu r)$ is the single-scattering propagator, which is the product of two complex-conjugate average Green's functions of the scalar field, where $\mu = \mu_s + \mu_a$ is the extinction coefficient, which is the sum of the scattering, μ_s, and absorption, μ_a, coefficients. Equation (2) is written in the ladder approximation under the weak-scattering condition $\lambda \ll l_s = \mu_s^{-1}$ and using the optical theorem for the scalar field,

$$\mu_s = \frac{k_0^4}{(4\pi)^2}\int d\Omega_f G(\mathbf{k}_f - \mathbf{k}_i),$$

where $G(\mathbf{k})$ is the Fourier transform of the correlation function of fluctuations of the permittivity given by the expression

$$G(\mathbf{k}) = \int d(\mathbf{r} - \mathbf{r}_0)e^{-i\mathbf{k}\cdot(\mathbf{r}-\mathbf{r}_0)}\langle\delta\varepsilon(\mathbf{r})\delta\varepsilon^*(\mathbf{r}_0)\rangle.$$

The normalization of $G(\mathbf{k})$ gives the phase function

$$p\left(\mathbf{k}_f - \mathbf{k}_i\right) = G(\mathbf{k}_f - \mathbf{k}_i)/\int d\Omega_f G(\mathbf{k}_f - \mathbf{k}_i),$$

which is a function of the angle θ between the vectors $\mathbf{k}_i$ and $\mathbf{k}_f$.

The backscattering intensity in the single-scattering approximation $J^{(1)}(s_i, s_f)$ is obtained by substituting the first term on the right-hand side of the Bethe–Salpeter equation into Eq. (1). The substitution of the entire iterative series for the Bethe–Salpeter equation (2) into Eq. (1) gives the scattering intensity in the form of the series in the scattering order [13, 22, 25]:

$$J(s_i, s_f) = \sum_{n=1}^\infty J^{(n)}(s_i, s_f),$$

where the single- and double-scattering terms have the form

$$J^{(1)}(s_i, s_f) = 4\pi(\mu_s/\mu)(s_f + s_i)^{-1}p(\mathbf{k}_f - \mathbf{k}_i),$$

$$J^{(2)}(s_i, s_f) = 4\pi\mu_s^2\int_0^\infty dz_1 \int_{z_2>0} d\mathbf{r}_2\Lambda(r_{21}) \times p(\mathbf{k}_{21} - \mathbf{k}_i)p(\mathbf{k}_f - \mathbf{k}_{21})e^{-\mu(s_i z_1 + s_f z_2)}.$$

The nth-order scattering term with $n \geq 3$ is given by the multiple integral

$$J^{(n)}(s_i, s_f) = 4\pi\mu_s^n\int_0^\infty dz_1\int d\mathbf{r}_2 \ldots \int d\mathbf{r}_n\Lambda(r_{21}) \times p(\mathbf{k}_{21} - \mathbf{k}_i)\prod_{j=2}^{n-1}\Lambda(r_{j+1j})p(\mathbf{k}_{j+1j} - \mathbf{k}_{jj-1}) \times H(z_j)H(z_n)p(\mathbf{k}_f - \mathbf{k}_{nn-1})e^{-\mu(s_i z_1 + s_f z_n)}. \quad (3)$$

Here, the Heaviside step functions $H(z)$ ensure the inclusion of scattering events only inside the semi-infinite randomly inhomogeneous medium.

For the Monte Carlo calculation of the contribution from the nth-order scattering to the intensity by Eq. (3), we repeatedly perform the inverse transform determining the relation between $\mathbf{r}_1, \mathbf{r}_2, \ldots, \mathbf{r}_n$ and functions depending on them with uniformly distributed random numbers. This procedure for a homogeneous system was described in detail in [13, 22]. As a result, averaging over a sample of N_{ph} incident photons for

the case of the normal incidence of a laser beam on the multilayer system gives

$$J^{(n)}(1,s_f) \simeq \sum_{i=1}^{N_{\rm ph}} \frac{W_n^{(i)}}{N_{\rm ph}} p\left(\mathbf{k}_f - \mathbf{k}_{nn-1}^{(i)}\right) e^{-\mu s_f z_n^{(i)}}.$$

The weights $W_n^{(i)}$ are the random values of multiple spatial integrals obtained in the nth order of the iterative solution of the Bethe–Salpeter equation and are calculated by simulating a stochastic sequence (photon trajectory) of the scattering points $\mathbf{r}_1,\ldots,\mathbf{r}_n$.

The Monte Carlo method is widely used for the simulation of photon migration in tissues and tissue phantoms primarily with the known MCML method [26], where photons leaving the scattering medium contribute to the signal. This procedure requires a rather large sample because the number of photons randomly leaving the medium with a particular geometry can constitute a very small fraction of the intensity of incident light. In the modification of the MCML method used in this work, each photon contributes to the detected signal in each scattering event until it leaves the medium. In this case, the size of the sample and, correspondingly, the computation time necessary for obtaining stable results decrease significantly.

INVERSE TRANSFORM METHOD FOR A MULTILAYERED MEDIUM

The simulation of photon propagation in the medium is performed in several steps. In the first step, the photon motion direction is determined. The normal incidence of a plane wave is considered. The scattering direction in all events is random and is determined by generating a random number distributed uniformly in the interval [0, 1] and performing the inverse transform of the Henyey–Greenstein model phase function [1]:

$$p_{\rm HG}(\cos\theta) = (4\pi)^{-1}(1-g^2)(1+g^2-2g\cos\theta)^{-3/2},$$

where $g = \langle\cos\theta\rangle$ is the scattering anisotropy parameter. It is assumed that the azimuth angle is uniformly distributed. In the second step of the simulation, the distance that the photon passes to the next scattering event is determined by generating another uniformly distributed random number ξ and applying the inverse transform generalized for the multilayer system. Since the photon can be located in any part of the system, this distance depends on the position of the photon and the angle determined in the preceding step.

The inverse transform procedure for the bilayer medium was described in detail in [13]. In this work, we study a more realistic model of the human head consisting of four layers: skin, skull, CSF, and brain. Below, we construct the distribution function of the path length of the photon to the next scattering event and perform the inverse transform for the system with an arbitrary number of layers. In the proposed algorithm, we use a new order of application of the inverse transform to the spatial and angular variables; the reverse order is efficient for the multilayer system because of the cylindrical symmetry since the random free path of the photon in this case is determined in a given direction.

The optical parameters in the inhomogeneous medium under study depend on the position of a photon, i.e., on the Cartesian coordinate z on the normal to the boundaries, in particular, $\mu = \mu(z)$. The layers from the outer to the inner are denoted by the letters A, B, C, and D and their thicknesses are T_A, T_B, T_C, and T_D. We introduce the brief notation $T_{AB} = T_A + T_B$ and $T_{ABC} = T_A + T_B + T_C$. Thus, layers A, B, C, and D occupy the regions $0 < z < T_A$, $T_A < z < T_{AB}$, $T_{AB} < z < T_{ABC}$, and $T_{ABC} < z < T$, respectively, where $T = T_A + T_B + T_C + T_D$ is the thickness of the entire four-layer system. To construct the inverse transform, we consider the layer D as the semi-infinite layer $T_{ABC} < z$, and the numerical calculations are performed with a finite T_D value but $T_D \gg T_{ABC}$.

Since the photon between two successive scattering events can move in a certain layer or intersect the interface between two layers and can approach the $z = 0$ boundary or move away from it, all these cases should be taken into account when constructing the cumulative distribution function and performing the inverse transform. In the system of k layers, there are $k(k+1)$ different types of photon paths between the successive scattering events; i.e., 20 different types of paths exist in the four-layer system under consideration. Thus, it is necessary to construct an algorithm for the determination of successive paths of the photon beginning with the point z_0. We describe in detail the case where the photon scattered at the point z_0 in layer A moves deeper into the medium; i.e., $\cos\theta > 0$, where θ is the angle between the z axis and the photon propagation direction. To describe a random distance traveled by the photon between two successive scattering events, we define the probability density function, as done in the MCML method [26]:

$$f(z) = \begin{cases} \dfrac{\mu_s(A)}{C\cos\theta}\exp\left(\dfrac{-\mu(A)}{\cos\theta}(z-z_0)\right), \\ \dfrac{\mu_s(B)}{C\cos\theta}\xi_A\exp\left(\dfrac{-\mu(B)}{\cos\theta}(z-T_A)\right), \\ \dfrac{\mu_s(C)}{C\cos\theta}\xi_A\xi_B\exp\left(\dfrac{-\mu(C)}{\cos\theta}(z-T_{AB})\right), \\ \dfrac{\mu_s(D)}{C\cos\theta}\xi_A\xi_B\xi_C\exp\left(\dfrac{-\mu(D)}{\cos\theta}(z-T_{ABC})\right). \end{cases} \quad (4)$$

Rows on the right-hand sides of this and other "multilayer" formulas from top to bottom refer to layers A, B, C, and D, and

$$\xi_A = \exp\left(\frac{-\mu(A)}{\cos\theta}(T_A - z_0)\right),$$

$$\xi_B = \exp\left(\frac{-\mu(B)}{\cos\theta}T_B\right), \quad \xi_C = \exp\left(\frac{-\mu(C)}{\cos\theta}T_C\right).$$

Integrating probability density (4), we obtain the cumulative distribution function F, which generates a uniformly distributed random number $\xi = F(z, z_0)$. The inverse transform gives

$$z(\xi) = \begin{cases} z_0 - \dfrac{\cos\theta}{\mu(A)}\ln\left(1 - \dfrac{C\xi'_A\xi}{C_1}\right), \\ T_A - \dfrac{\cos\theta}{\mu(B)}\ln\left(1 - \dfrac{C\xi'_B}{C_2}(\xi - \xi^B_{\text{crit}})\right), \\ T_{AB} - \dfrac{\cos\theta}{\mu(C)}\ln\left(1 - \dfrac{C\xi'_C}{C_3}(\xi - \xi^C_{\text{crit}})\right), \\ T_{ABC} - \dfrac{\cos\theta}{\mu(D)}\ln\left(1 - \dfrac{C}{C_4}(\xi - \xi^D_{\text{crit}})\right). \end{cases}$$

The quantities ξ^B_{crit}, ξ^C_{crit}, and ξ^D_{crit} are the ξ values at which the photon reaches the interface between layer B, C, or D and the preceding layer. In terms of $\xi'_i = 1 - \xi_i$, the normalization constant has the form

$$C = C_1 + C_2 + C_3 + C_4,$$

$$C_1 = A_\mu\xi'_A, \quad C_2 = B_\mu\xi_A\xi'_B,$$

$$C_3 = C_\mu\xi_A\xi_B\xi'_C, \quad C_4 = D_\mu\xi_A\xi_B\xi_C.$$

Here, the albedos of the layers are

$$A_\mu = \mu_s(A)/\mu(A), \quad B_\mu = \mu_s(B)/\mu(B),$$

$$C_\mu = \mu_s(C)/\mu(C), \quad D_\mu = \mu_s(D)/\mu(D).$$

The values of the random number ξ corresponding to the boundaries of the layers can be represented in the form

$$\xi_{\text{crit}} = \frac{1}{C}\times\begin{cases} C_1, \\ C_1 + C_2, \\ C_1 + C_2 + C_3. \end{cases}$$

Expression (4) for the probability density of the mean free path of the photon in the four-layer system can be generalized to the case of scattering in the system of k plane layers $A_1, A_2, \ldots, A_k$ with finite thicknesses $T_1, T_2 \ldots, T_{k-1}$ and $T_k = \infty$. The probability densities in the first and nth layers for $n \geq 2$ are given by the expressions

$$f_1(z) = \frac{\mu_s(A_1)}{C\cos\theta}\exp\left(\frac{-\mu(A_1)}{\cos\theta}(z - z_0)\right), \quad n = 1, \quad (5)$$

$$f_n(z) = \frac{\mu_s(A_n)}{C\cos\theta}\prod_{i=1}^{n-1}\xi_i\exp\left(\frac{-\mu(A_n)}{\cos\theta}\left(z - \sum_{j=1}^{n-1}T_j\right)\right). \quad (6)$$

Here, the normalization constant is given by the formula

$$C = \sum_{i=1}^{k}C_i, \quad C_i = \frac{\mu_s(A_i)}{\mu(A_i)}\xi'_i\prod_{j=0}^{i-1}\xi_j, \quad 1 \leq i \leq k,$$

$$\xi_1 = \exp\left(\frac{-\mu(A_1)}{\cos\theta}(T_1 - z_0)\right),$$

$$\xi_i = \exp\left(\frac{-\mu(A_i)}{\cos\theta}T_i\right), \quad i \geq 2,$$

$\xi'_i = 1 - \xi_i$, and we formally set $\xi_0 = 1$ and $\xi_k = 0$. Integrating probability densities (5) and (6), we obtain the cumulative distribution function, and applying the inverse transform to it, we arrive at the dependence of the coordinate z of the photon after the scattering event on the uniformly distributed random number ξ:

$$z(1) = z_0 - \frac{\cos\theta}{\mu(A_1)}\ln\left(1 - \frac{C\xi'_1\xi'}{C_1}\right),$$

$$z(n) = \sum_{i=1}^{n-1}T_i - \frac{\cos\theta}{\mu(A_n)}\ln\left(1 - \frac{C\xi'_n}{C_n}(\xi - \xi^{A_n}_{\text{crit}})\right),$$

$$z(k) = \sum_{i=1}^{k-1}T_i - \frac{\cos\theta}{\mu(A_k)}\ln\left(1 - \frac{C}{C_k}(\xi - \xi^{A_k}_{\text{crit}})\right).$$

Here, $2 \leq n < k$ and $\xi^{A_n}_{\text{crit}} = \sum_{i=1}^{n}C_i/C$. The above expressions make it possible to simulate the distance traveled by the photon in the system of k layers with different optical characteristics.

Below, we also report the results of our Monte Carlo calculations for the case of the penetration of light into the biological tissue at a random angle θ_i to the surface governed by a normal distribution with the standard deviation σ.

SIMULATION RESULTS

In this section, we report the calculated backscattering intensity of laser radiation of the near infrared range in the four-layer medium. The optical parameters of the layers taken for the skin–skull–CSF–brain system from [6, 27] are presented in Table 1. The anisotropy parameter in all performed calculation was $g = 0.9$. According to the data on the thicknesses of the layers for the human head, we took the thicknesses $T_A = 3$ mm, $T_B = 7$ mm, and $T_C = 3$ mm for the skin, skull, and CSF layers, respectively. In this case, the brain layer occupied the remaining place in the system and had a thickness of $T_D = 150$ mm.

The Monte Carlo simulation was performed both with the traditional approach to the calculation of the inverse transform for the cumulative distribution function of the mean free path of the photon described previously and with the modification proposed in [13]

Table 1. Absorption coefficients μ_a and reduced scattering coefficients μ_s' of four tissues at four wavelengths

	Wavelength λ							
	750 nm		850 nm		950 nm		1050 nm	
	μ_a, mm^{-1}	μ_s', mm^{-1}	μ_a, mm^{-1}	μ_s', mm^{-1}	μ_a, mm^{-1}	μ_s', mm^{-1}	μ_a, mm^{-1}	μ_s'
Brain	0.036	0.859	0.106	0.762	0.114	0.622	0.118	0.525
Skull	0.006	1.974	0.013	1.876	0.019	1.757	0.019	1.665
Blood	0.530	0.725	0.720	0.649	0.930	0.650	0.560	0.645
Skin	0.046	1.535	0.038	1.485	0.030	1.625	0.022	1.695

generalized to the four-layer system. The medium in the simulation occupied the half-space $z \geq 0$. Laser radiation penetrated into this medium at the point (0, 0, 0) on its surface and moved along the z axis deeper into the medium. Multiple scattering in the four-layer medium resulted in the appearance of backscattering whose intensity was calculated at a point on the $z = 0$ surface at different distances ρ from the

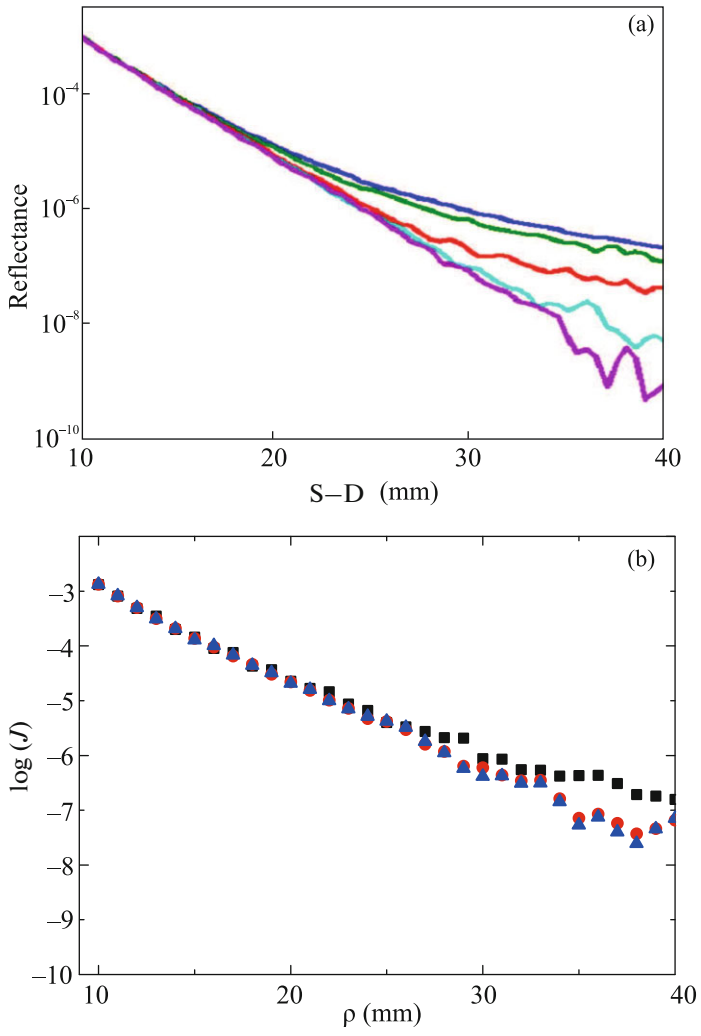

Fig. 1. (Color online) Backscattering intensity at a wavelength of λ = 750 nm for the four-layer model of the human head including 3-mm skin, 7-mm skull, and 2-mm cerebrospinal fluid versus the source–detector distance. (a) Plot from [6] for 100-mm brain. (b) Results of this work for 150-mm brain and the blood concentration in the cerebrospinal fluid of (squares) 0, (circles) 50, and (triangles) 100%.

point of penetration of the laser beam into the medium. Contributions to the backscattering intensity decrease with increasing scattering order, and we took the maximum scattering order $n = 5\times10^5$. The size of the sample was taken $N_{ph} = 10^6$–10^7 to ensure a sufficient accuracy.

Figure 1 shows the simulated dependence of the backscattering intensity on the distance between the source and the detector for the skin–skull–CSF–brain system. The data presented in Fig. 1a are taken from [6], where the localized propagation of blood in the CSF layer was considered. The data presented in Fig. 1b were obtained for different blood concentrations n in the CSF layer. The line in Fig. 1b for $n = 0\%$, i.e., the complete absence of blood in the CSF layer, corresponds to the upper line in Fig. 1a, whereas the line in Fig. 1b for $n = 100\%$, i.e., the complete filling of the CSF layer with blood, corresponds to the lower line in Fig. 1a. Figures 2a and 2b also show the dependences of the backscattering intensity on the distance between the source and the detector for the skin–skull–CSF–brain system with a skull thickness of 5 and 10 mm, respectively. These calculations were carried out in order to determine the effect of the screening of deep layers by the skull and to estimate the significance of the depth of the location of focus of hemorrhage in the head. According to the simulation, the closer the CSF layer to the surface of the head, the more noticeable the appearance of blood in this layer. In particular, the difference in the backscattering intensity in the case of the 10-mm skull can be determined only at sufficiently long distances between the source and the detector of laser radiation (>30 mm), whereas this difference in the case of the 5-mm skull is seen at smaller distances (>17 mm).

To determine the effect of the angular spread of penetration of the photon to the multilayer system, we performed calculations for several angular distributions: (i) normal incidence, (ii) uniform distribution in the angular interval $[0, \pi/2]$, and (iii) normal distribution with zero mean and standard deviations σ of $\pi/6$ and $\pi/90$. The first standard deviation corresponds to the characteristic deviation caused by the measurement error, and the second standard deviation corresponds to the characteristic angle of the radiation cone of a waveguide. The results are presented in Fig. 3. It is seen that the results in the case of the normal incidence of photons on the medium are almost identical to those for the case $\sigma = \pi/90$. The uniform angular distribution gives the lowest backscattering intensity, whereas the curve for $\sigma = \pi/6$ is between the curves for $\sigma = \pi/90$ and the curves obtained with the uniform angular distribution. The simulation shows that the variation of the angular spread of radiation changes the backscattering intensity at distances between the source and the detector that provide the most complete information on the structure of the medium under consideration.

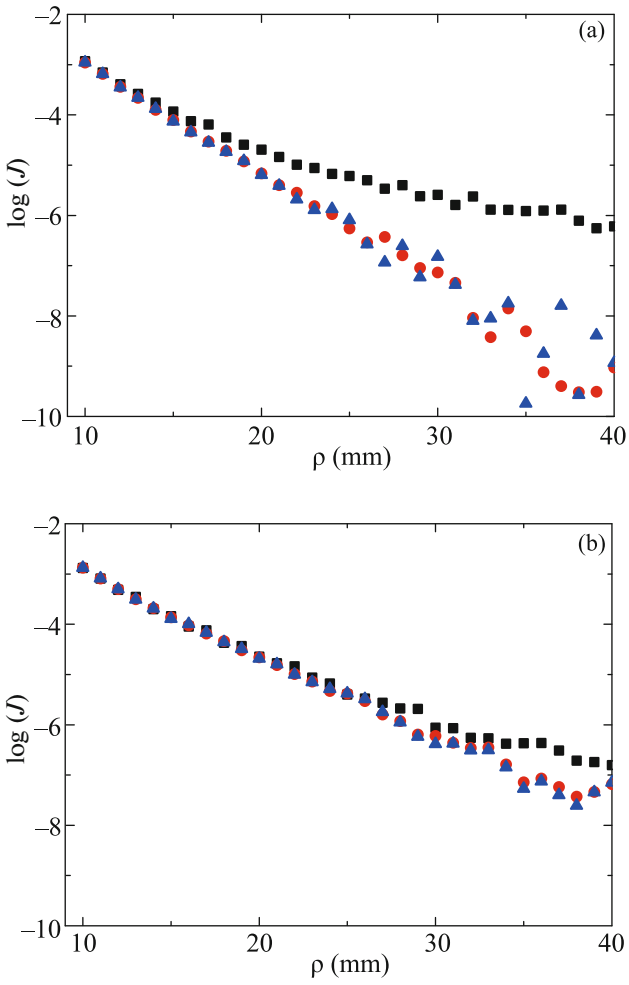

Fig. 2. (Color online) Backscattering intensity at a wavelength of $\lambda = 750$ nm and an anisotropy parameter of $g = 0.9$ for the four-layer model of the human head consisting of 3-mm skin, (a) 5- or (b) 10-mm skull, 2-mm cerebrospinal fluid, and 150-mm brain versus the source–detector distance at the blood concentration in the cerebrospinal fluid (squares) 0, (circles) 50, and (triangles) 100%.

The alternative order of the inverse transform proposed in [13] was also considered in application to the four-layer system, but the results obtained with different orders are within the error of the calculation, as in the case of the bilayer system.

CONCLUSIONS

To summarize, the backscattering intensity of infrared laser radiation has been calculated for a randomly inhomogeneous four-layer biological tissue. The calculations have been performed for the skin–skull–cerebrospinal fluid–brain model system, which

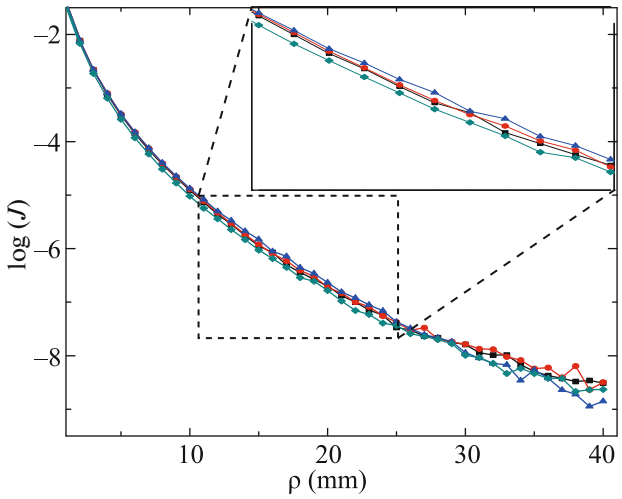

Fig. 3. (Color online) Backscattering intensity at a wavelength of $\lambda = 750$ nm and an anisotropy parameter of $g = 0.9$ for the four-layer model of the human head including 3-mm skin, 7-mm skull, 2-mm cerebrospinal fluid, and 150-mm brain versus the source–detector distance for (triangles) normal incidence of radiation on the medium, (circles) Gaussian distribution of radiation with $\sigma = \pi/90$, (squares) Gaussian distribution of radiation with $\sigma = \pi/6$, and (diamonds) uniform distribution of radiation.

is more appropriate for the simulation of the human head than the simplified bilayer skull–brain biological model considered in our previous work [13]. The Bethe–Salpeter equation in the ladder approximation has been used to simulate radiation transport in the biological tissue taking into account multiple scattering. The representation of its solution in the form of a series in scattering orders, where each term is a multiple integral, allows us to use the Monte Carlo method to calculate the terms of the series. The Henyey–Greenstein model phase function with the anisotropy parameter $g = 0.9$ has been used to take into account the anisotropy of radiation scattering in the biological tissue. The calculations have been performed with our modification of the known MCML method [26], which differs in the method of detection of photons [22]. The mean free path of the photon has been simulated with both the traditional MCML method and its modification proposed in [13]. The calculated dependences of the intensity of backscattered infrared radiation on the distance between the source and the detector located directly on the human head are very sensitive to the blood concentration in the cerebrospinal fluid layer. This allows the application of comparatively inexpensive optical methods for fast field diagnosis of traumatic injuries and hemorrhages in the human head and in other multilayer biological tissues.

FUNDING

This work was supported by the Russian Science Foundation, project no. 23-22-00035, https://rscf.ru/project/23-22-00035/.

CONFLICT OF INTEREST

The authors declare that they have no conflicts of interest.

REFERENCES

1. V. V. Tuchin, *Tissue Optics: Light Scattering Methods and Instruments for Medical Diagnostics* (IPR Media, Moscow, 2021; SPIE, Bellingham, 2015).
2. S. L. Jacques, Phys. Med. Biol. **58**, R37 (2013).
3. D. J. Davies, Z. Su, M. T. Clancy, S. J. Lucas, H. Dehghani, A. Logan, and A. Belli, J. Neurotrauma **32**, 933 (2015).
4. A. Sabeeh and V. V. Tuchin, J. Biomed. Photon. Eng. **6**, 040201 (2020).
5. A. P. Tran, S. Yan, and Q. Fang, Neurophotonics **7**, 015008 (2020).
6. R. Francis, B. Khan, G. Alexandrakis, J. Florence, and D. MacFarlane, Biomed. Opt. Express **6**, 3256 (2015).
7. E. S. Papazoglou, M. S. Weingarten, L. Zubkov, M. Neidrauer, L. Zhu, S. Tyagi, and K. Pourrezaei, J. Biomed. Opt. **13**, 044005 (2008).
8. E. S. Papazoglou, M. T. Neidrauer, L. Zubkov, M. S. Weingarten, and K. Pourrezaei, J. Biomed. Opt. **14**, 064032 (2009).
9. E. Zinchenko, N. Navolokin, A. Shirokov, et al., Biomed. Opt. Express **10**, 4003 (2019).
10. F. Scholkmann, S. Kleiser, A. J. Metz, R. Zimmermann, J. Mata Pavia, U. Wolf, and M. Wolf, Neuroimage **85**, 6 (2014).
11. H. Liu, D. A. Boas, Y. Zhang, A. G. Yodh, and B. Chance, Phys. Med. Biol. **40**, 1983 (1995).
12. O. Pucci, V. Toronov, and K. St. Lawrence, Appl. Opt. **49**, 6324 (2010).
13. V. L. Kuzmin, Yu. A. Zhavoronkov, S. V. Ul'yanov, and A. Yu. Valkov, J. Exp. Theor. Phys. **134**, 661 (2022).
14. J. Zhao, H. S. Ding, X. L. Hou, C. L. Zhou, and B. Chance, J. Biomed. Opt. **10**, 024028 (2005).
15. V. Ntziachristos and B. Chance, Med. Phys. **28**, 1115 (2001).
16. A. Torricelli, D. Contini, A. Pifferi, M. Caffini, R. Re, L. Zucchelli, and L. Spinelli, Neuroimage **85**, 28 (2014).
17. H. Wabnitz, J. Rodriguez, I. Yaroslavsky, A. Yaroslavsky, and V. V. Tuchin, in *Handbook of Optical Biomedical Diagnostics. Light-Tissue Interaction,* 2nd ed. (SPIE Press, Bellingham, Washington, 2016), Vol. 1, p. 401.
18. T. Durduran, R. Choe, J. P. Culver, L. Zubkov, M. J. Holboke, J. Giammarco, B. Chance, and A. G. Yodh, Phys. Med. Biol. **47**, 2847 (2002).

19. M. A. Franceschini, S. Thaker, G. Themelis, K. K. Krishnamoorthy, H. Bortfeld, S. G. Diamond, D. A. Boas, K. Arvin, and P. E. Grant, Pediatr. Res. **61**, 546 (2007).
20. S. Mahmoodkalayeh, M. A. Ansari, and V. V. Tuchin, Biomed. Opt. Express **10**, 2795 (2019).
21. M. S. Cano-Velázquez, N. Davoodzadeh, D. Halaney, C. R. Jonak, D. K. Binder, J. Hernández-Cordero, and G. Aguilar, Biomed. Opt. Express **10**, 3369 (2019).
22. V. L. Kuz'min, A. Yu. Val'kov, and L. A. Zubkov, J. Exp. Theor. Phys. **128**, 396 (2019).
23. V. L. Kuzmin, V. P. Romanov, and E. V. Aksenova, Phys. Rev. E **65**, 016601 (2001).
24. T. M. Nieuwenhuizen and J. M. Luck, Phys. Rev. E **48**, 569 (1993).
25. V. L. Kuzmin, M. T. Neidrauer, D. Diaz, and L. A. Zubkov, J. Biomed. Opt. **20**, 105006 (2015).
26. L. Wang, S. L. Jacques, and L. Q. Zheng, Comput. Meth. Prog. Biol. **47**, 131 (1995).
27. A. N. Bashkatov, E. A. Genina, V. I. Kochubey, and V. V. Tuchin, Proc. SPIE **6163**, 616310 (2006).

Translated by R. Tyapaev